

# Preparation and characterization of Nd<sub>2</sub>O<sub>3</sub> nanostructures via a new facile solvent-less route

Sobhan Mortazavi-Derazkola<sup>1</sup> · Sahar Zinatloo-Ajabshir<sup>1</sup> · Masoud Salavati-Niasari<sup>1</sup>

Received: 29 January 2015 / Accepted: 22 April 2015 / Published online: 29 April 2015  
© Springer Science+Business Media New York 2015

**Abstract** Neodymium oxide (Nd<sub>2</sub>O<sub>3</sub>) nanostructures were synthesized via a novel facile solvent-less route. Nanostructures were prepared by heat treatment in air at 900 °C for 5 h, using [Nd L(NO<sub>3</sub>)<sub>2</sub>]NO<sub>3</sub> (L = bis-(2-hydroxy-1-naphthaldehyde)-butanediamine Schiff base ligand), as precursor, which was obtained by a solvent-free solid–solid reaction from different molar ratios of neodymium nitrate and Schiff base ligand. The as-obtained nanostructures were characterized by means of techniques such as scanning electron microscopy, X-ray diffraction, transmission electron microscopy, thermo-gravimetric analysis, UV–Vis diffuse reflectance spectroscopy, energy dispersive X-ray microanalysis, and Fourier transform infrared spectroscopy. It was found that purity, morphology and particle size of the final Nd<sub>2</sub>O<sub>3</sub> could be dramatically affected via the calcination temperature and molar ratio of neodymium nitrate and Schiff base ligand. The photocatalyst activity of as-prepared nanostructured Nd<sub>2</sub>O<sub>3</sub> was also examined by degradation of rhodamine B as cationic dye under ultraviolet light irradiation.

## 1 Introduction

In the past decade, considerable attention has been paid to the preparation of nanostructured materials owing to their wide range of interesting and unique properties and important and significant potential applications [1–7]. Among

these nanometer-scale materials, neodymium oxide is well known as an important rare earth metal oxide with specific and unique optical and electrical properties, and has been widely investigated for applications in the luminescent and thermoluminescent materials, advanced materials, photonic, thin films, catalysts and protective coatings [8–13]. Until now, very limited numbers of synthetic routes have been documented in the literature to prepare nanostructured neodymium oxide such as microemulsion [14], solution-coprecipitation [15], gel combustion [16], hydrothermal [17], thermal decomposition [18] and hydrogen plasma-metal reaction [12].

Various nanostructured metal oxides have been synthesized by the thermal decomposition the organometallic molecular route as an appropriate synthetic approach. This approach as simple, reliable and cost effective synthetic route to the production of pure and uniform nanometer-scale materials does not need special apparatus, complicated procedures and severe reaction conditions, which can limit the large-scale synthesis of the nanomaterials. On the other hand, solvent-free synthetic routes have attracted considerable attention in the field of green chemistry, and many solvent-less synthetic routes for organic compounds have been introduced. From the viewpoint of green chemistry, we succeeded in synthesizing rare earth metal complexes by solvent-free solid–solid reactions, and here we present the novel synthesis of [Nd L(NO<sub>3</sub>)<sub>2</sub>]-NO<sub>3</sub> (L = bis-(2-hydroxy-1-naphthaldehyde)-butanediamine Schiff base ligand) via simple solvent-free reactions using different molar ratios of neodymium nitrate and Schiff base ligand, and then [Nd L(NO<sub>3</sub>)<sub>2</sub>]NO<sub>3</sub> was utilized for preparing neodymium oxide nanostructures via a thermal treatment route. To the best of our knowledge, investigations on the preparation of nanostructured Nd<sub>2</sub>O<sub>3</sub> by utilizing [Nd L(NO<sub>3</sub>)<sub>2</sub>]NO<sub>3</sub> have not been reported to date.

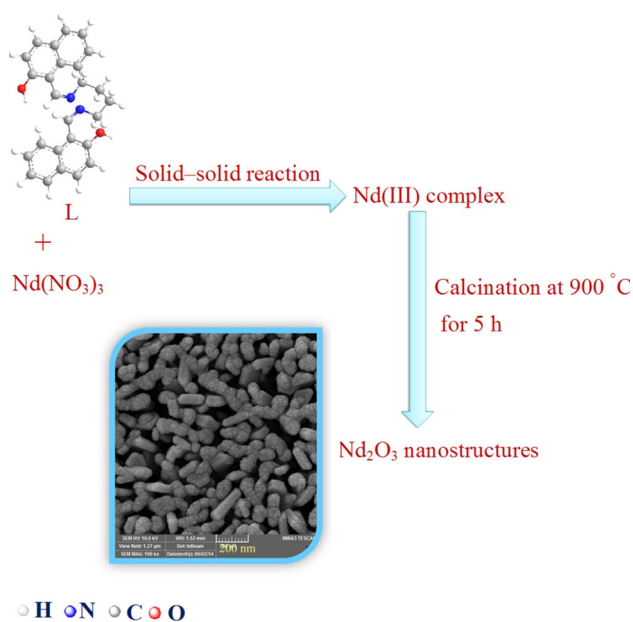
✉ Masoud Salavati-Niasari  
salavati@kashanu.ac.ir

<sup>1</sup> Institute of Nano Science and Nano Technology, University of Kashan, P. O. Box 87317-51167, Kashan, Islamic Republic of Iran

## 2 Experimental

### 2.1 Materials and characterization

In this study, 2-hydroxy-1-naphthaldehyde, neodymium nitrate [Nd(NO<sub>3</sub>)<sub>3</sub>·6H<sub>2</sub>O], 1,4-diaminobutane, methanol, ethyl acetate and chloroform, were purchased from Merck Co. and were used as received. Transmission electron microscope (TEM) images of neodymium oxide were obtained on a JEM-2100 with an accelerating voltage of 200 kV equipped with a high resolution CCD Camera. A Tescan mira3 field emission scanning electron microscope (FESEM) was utilized to visualize FESEM images of



**Scheme 1** Schematic diagram of the synthesis of Nd<sub>2</sub>O<sub>3</sub> micro/nanostructures

neodymium oxide. Thermogravimetric–differential thermal analysis (TG–DTA) was investigated by a thermal gravimetric analysis instrument (Shimadzu TGA-50H) with a flow rate of 20.0 ml min<sup>-1</sup> and a heating rate of 10 °C min<sup>-1</sup>. The energy dispersive spectrometry (EDS) analysis was studied by XL30, Philips microscope. Fourier transform infrared spectra were recorded using a Magna-IR, spectrometer 550 Nicolet in KBr pellets in the range of

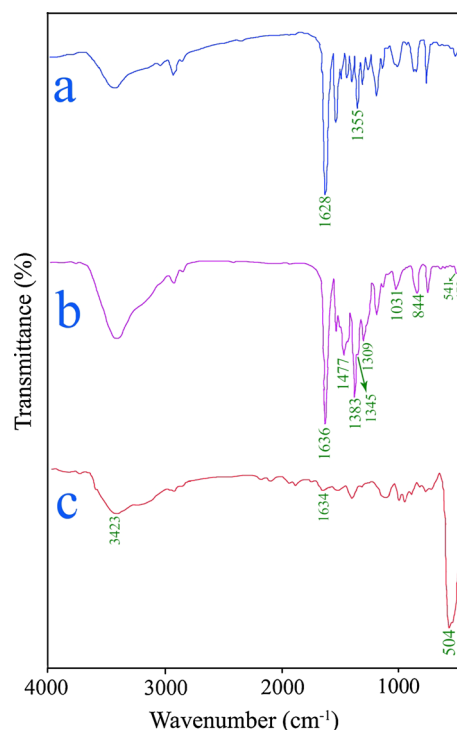


**Fig. 1** FT-IR spectra of *a* Schiff base ligand (L), *b* Nd(III) complex, and *c* Nd<sub>2</sub>O<sub>3</sub> nanoparticles obtained from Nd(III) complex in molar ratio of 1:1 by thermal treatment at 900 °C for 5 h

**Table 1** Preparation conditions of Nd<sub>2</sub>O<sub>3</sub> samples

Sample No.	Precursor	Molar ratio of Nd(NO <sub>3</sub> ) <sub>3</sub> ·6H <sub>2</sub> O/ Schiff base ligand (L)	Calcination temperature (°C)	Figure of SEM images
1	Nd(III)complex	1:1	500	5a
2	Nd(III)complex	1:1	600	5b
3	Nd(III)complex	1:1	700	5c
4	Nd(III)complex	1:1	800	6a
5	Nd(III)complex	1:1	900	6b and 7b
6	Nd(III)complex	1:0.5	900	7a
7	Nd(III)complex	1:2	900	7c
8	Nd(III)complex	1:3	900	8a
9	Nd(III)complex	1:4	900	8b
10 <sup>a</sup>	Nd(NO <sub>3</sub> ) <sub>3</sub> ·6H <sub>2</sub> O	–	900	8c

<sup>a</sup> Blank test, in the absence of Schiff base ligand (L)

400–4000  $\text{cm}^{-1}$ . The electronic spectra of the neodymium oxide were obtained on a Scinco UV–Vis scanning spectrometer (Model S-4100). Powder X-ray diffraction (XRD) patterns were collected with a diffractometer of Philips Company with X'PertPro monochromatized Cu K $\alpha$  radiation ( $\lambda = 1.54 \text{ \AA}$ ).

## 2.2 Synthesis of bis-(2-hydroxy-1-naphthaldehyde)-butanediamine Schiff base ligand (L)

To synthesize of Schiff base ligand (L), 0.06 mol of 2-hydroxy-1-naphthaldehyde dissolved in methanol (30 ml) was added drop-wise to a 1,4-diaminobutane solution (0.03 mol) in 30 ml of methanol. The mixture was refluxed for 3 h. The yellow precipitate was separated by filtration, washed and air-dried. It was then recrystallized from methanol. The as-synthesized ligand was characterized using FT-IR.

## 2.3 Synthesis of the Nd(III) complex

[Nd(NO $_3$ ) $_3$ ·6H $_2$ O] and Schiff base ligand (L) were mixed and ground for 15 min in an agate mortar at room temperature in a [Nd(NO $_3$ ) $_3$ ·6H $_2$ O] to (L) molar ratio of 1:0.5, 1:1, 1:2, 1:3 and 1:4. The identification of the resulting products was based on Fourier transform (FT-IR) spectrometer.

## 2.4 Synthesis of Nd $_2$ O $_3$ micro/nanostructures

Neodymium oxide micro/nanostructures were synthesized by subjecting 0.1 g of the as-prepared Nd(III) complex powders to heat treatment at (900 °C) in the air. An average temperature increase of 30 °C is recorded every minute, before the temperature reached 900 °C, and after keeping the thermal treatment at 900 °C for 5 h, it was

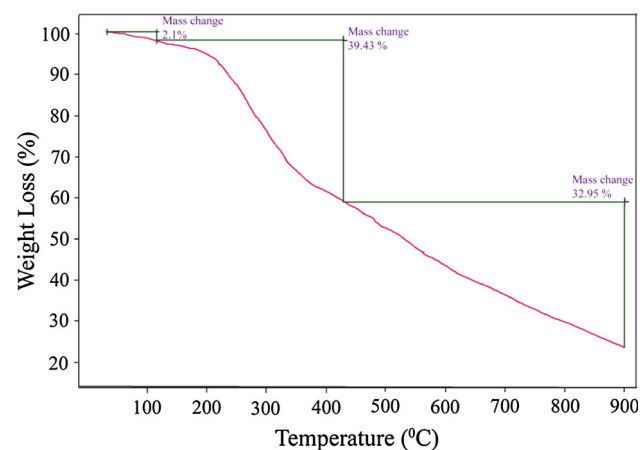
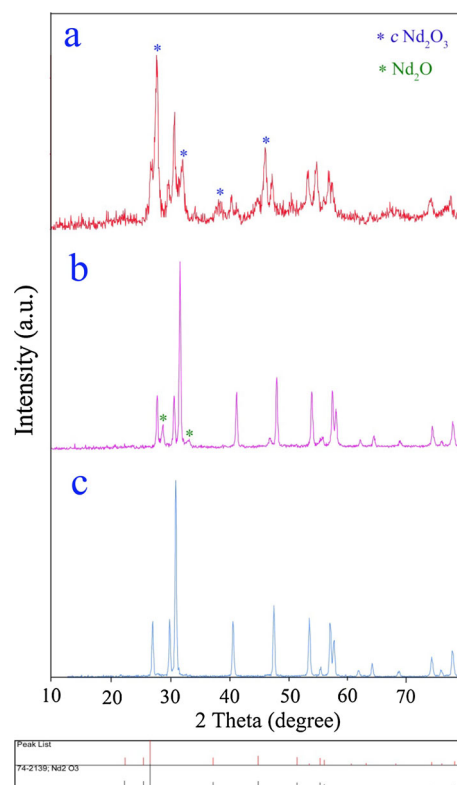


**Fig. 2** TGA of the Nd(III) complex precursor

allowed to cool to room temperature. Schematic diagram of formation of neodymium oxide micro/nanostructures is presented in Scheme 1. To study the effect of Schiff base ligand (L), a blank test was performed. In the blank test, 0.1 g of neodymium nitrate was subjected to heat treatment at 900 °C in the air. To investigate the effect of calcination temperature, the thermal treatment process of the solid precursor was carried out in the 500, 600, 700, 800 and 900 °C. The synthesis conditions of all samples were illustrated in Table 1. The as-prepared nanostructures were characterized by EDS, SEM, TEM, FT-IR, XRD, UV–Vis techniques.

## 2.5 Photocatalytic measurements

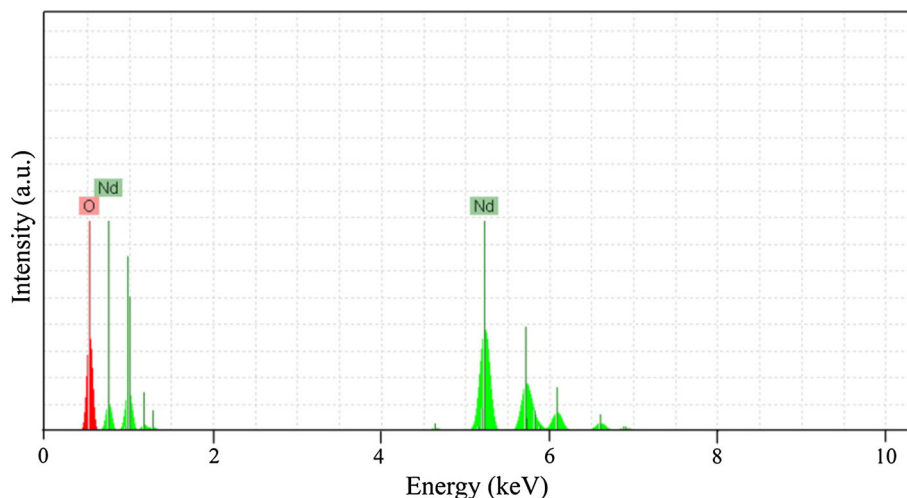
The photocatalytic activity of Nd $_2$ O $_3$  nanostructures obtained from sample no. 5 was examined by monitoring the degradation of rhodamine B solution as cationic dye in an aqueous solution. A quartz photocatalytic reactor was utilized to perform the degradation reaction. The photocatalytic degradation was carried out by utilizing 0.001 g of rhodamine B solution including 0.05 g of Nd $_2$ O $_3$  nanostructures at room temperature. To reach adsorption equilibrium, this mixture was aerated for 30 min. Later, the



**Fig. 3** XRD pattern of products obtained by thermal treatment of Nd(III) complex in molar ratio of 1:1 at *a* 700, *b* 800 and *c* 900 °C for 5 h

**Table 2** Preparation conditions and corresponding products

Sample No.	Calcination temperature (°C)	Composition of the products (XRD result)
3	700	Hexagonal Nd <sub>2</sub> O <sub>3</sub> + cubic Nd <sub>2</sub> O <sub>3</sub>
4	800	Hexagonal Nd <sub>2</sub> O <sub>3</sub> + NdO <sub>2</sub>
5	900	Hexagonal Nd <sub>2</sub> O <sub>3</sub>

**Fig. 4** EDS pattern of Nd<sub>2</sub>O<sub>3</sub> nanoparticles obtained by thermal treatment of Nd(III) complex in molar ratio of 1:1 at 900 °C for 5 h

mixture was placed inside the photoreactor in which the vessel was 40 cm away from the UV source of 400 W mercury lamps. To hinder UV leakage, the light source and quartz vessel were placed inside a black box that equipped with a fan. Aliquots of the mixture were taken at definite interval of times during the irradiation, and after centrifugation they were analyzed by a UV–Vis spectrometer. The rhodamine B degradation percentage was calculated as follow:

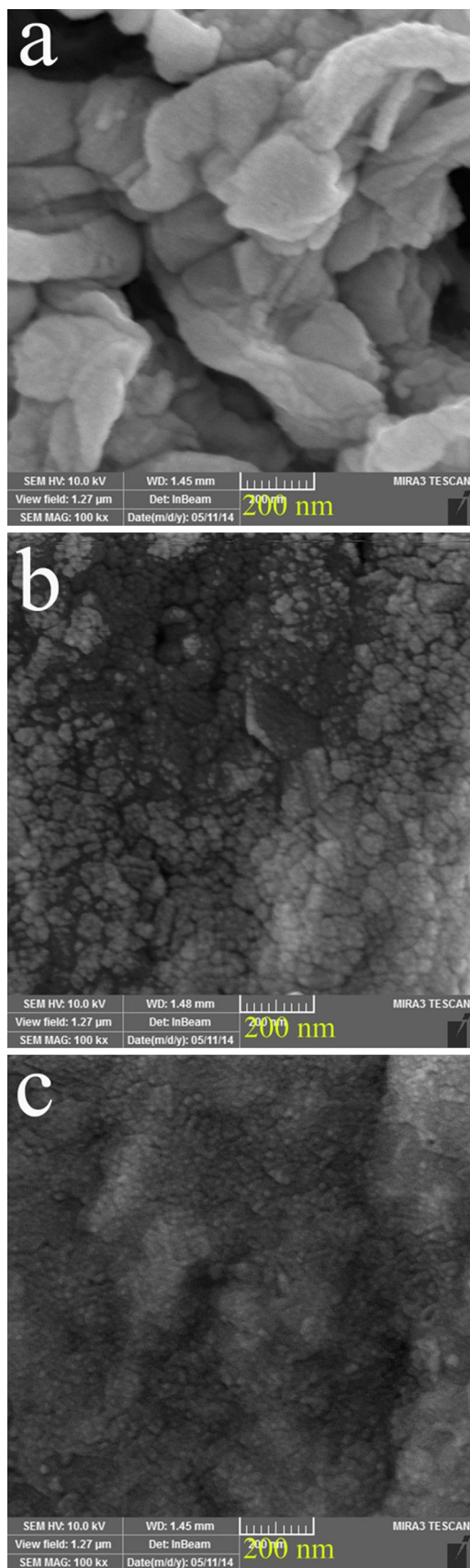
$$D.P. (t) = \frac{A_0 - A_t}{A_0} \times 100 \quad (1)$$

where  $A_0$  and  $A_t$  are the absorbance value of solution at 0 and  $t$  min, respectively.

### 3 Results and discussion

As described before, in this study, the bis-(2-hydroxy-1-naphthaldehyde)-butanediamine ligand was firstly prepared, to be utilized in the synthesis of Nd<sub>2</sub>O<sub>3</sub> nanostructures. FT-IR spectroscopy is well known as helpful and applicable device to understand the functional group of any organic molecule. The infrared spectra of Schiff base ligand, Nd(III) complex and Nd<sub>2</sub>O<sub>3</sub> nanostructures are shown in Fig. 1. Two peaks at 1628 and 1355 cm<sup>-1</sup> in Fig. 1a are attributed to the  $\nu(\text{C}=\text{N})$  of the azomethines and  $\nu(\text{Ar}-\text{O})$  of the phenolic hydroxyl substituent, respectively. The FT-IR spectrum of Nd(III) complex displays the

(L) ligand characteristic peaks with several different shifts because of complex formation. The FT-IR spectrum of the Nd(III) complex presents an increase in the C–O stretching frequency (10 cm<sup>-1</sup>) compared to the free (L) Schiff base ligand (Fig. 1b). This indicates that the coordination to the Nd(III) ion takes place by means of the oxygen atoms of the hydroxyl benzene of the (L) Schiff base ligand. This was additional proved by using the peak located at 541 cm<sup>-1</sup> which can be ascribed to  $\nu(\text{Nd}-\text{O})$  vibration (Fig. 1b). In comparison with the free (L) Schiff base ligand, the  $\nu(\text{C}=\text{N})$  peak in the Nd(III) complex shifted to 1636 cm<sup>-1</sup>. This blue shift (8 cm<sup>-1</sup>) shows a stronger double bond characteristic of the iminic bonds as well as contribution of the azomethines nitrogen atoms in the coordination [19]. This result was additional proved by using the peak located at 472 cm<sup>-1</sup> which might be related to  $\nu(\text{Nd}-\text{N})$  vibration (Fig. 1b). The different coordination modes of the nitrate groups to the neodymium metal were detected by the differences in the two bands  $|v_4 - v_1|$ . The FT-IR spectrum of the Nd(III) complex presents several peaks located at 1477 cm<sup>-1</sup> ( $v_1$ ), 1031 cm<sup>-1</sup> ( $v_2$ ), 843 cm<sup>-1</sup> ( $v_3$ ) and 1309 cm<sup>-1</sup> ( $v_4$ ) related to the coordinated nitrate ions (Fig. 1b). The difference between  $v_4$  and  $v_1$  is nearly 167 cm<sup>-1</sup> showing that the coordinated NO<sub>3</sub><sup>-</sup> ions in the complex may act as a bidentate ligand [20]. The ( $v_0$ ) free nitrate located at 1383 cm<sup>-1</sup> in the spectrum of the complex. The peak located at 3423 cm<sup>-1</sup> and a weak peak at 1634 cm<sup>-1</sup> ascribed to the  $\nu(\text{OH})$  stretching and bending vibrations, respectively, which shows the presence of



◀**Fig. 5** SEM images of the samples synthesized by thermal treatment of Nd(III) complex in molar ratio of 1:1 at **a** 500, **b** 600 and **c** 700 °C

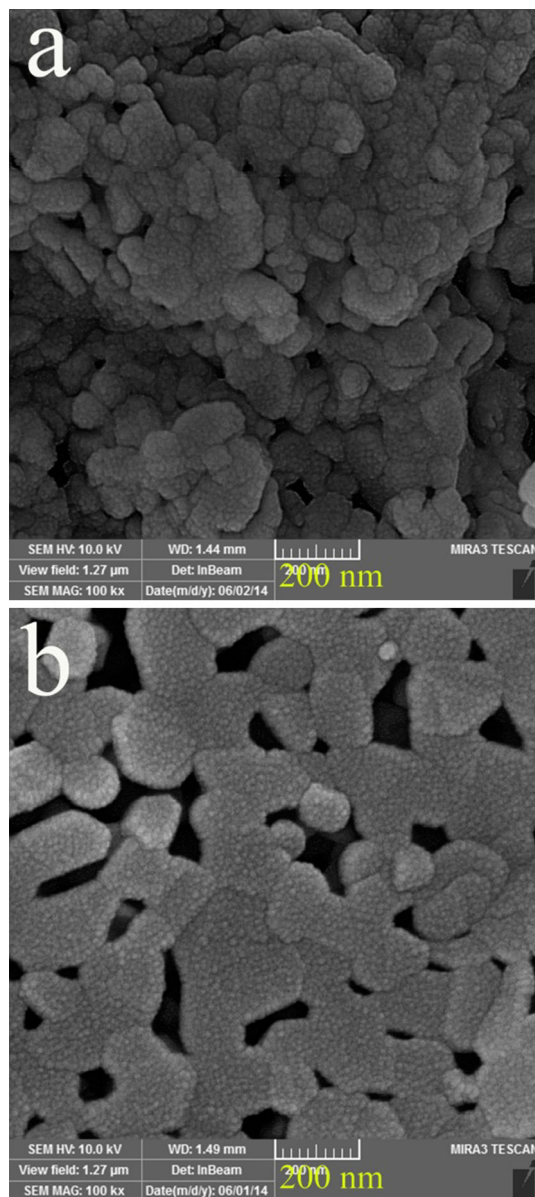
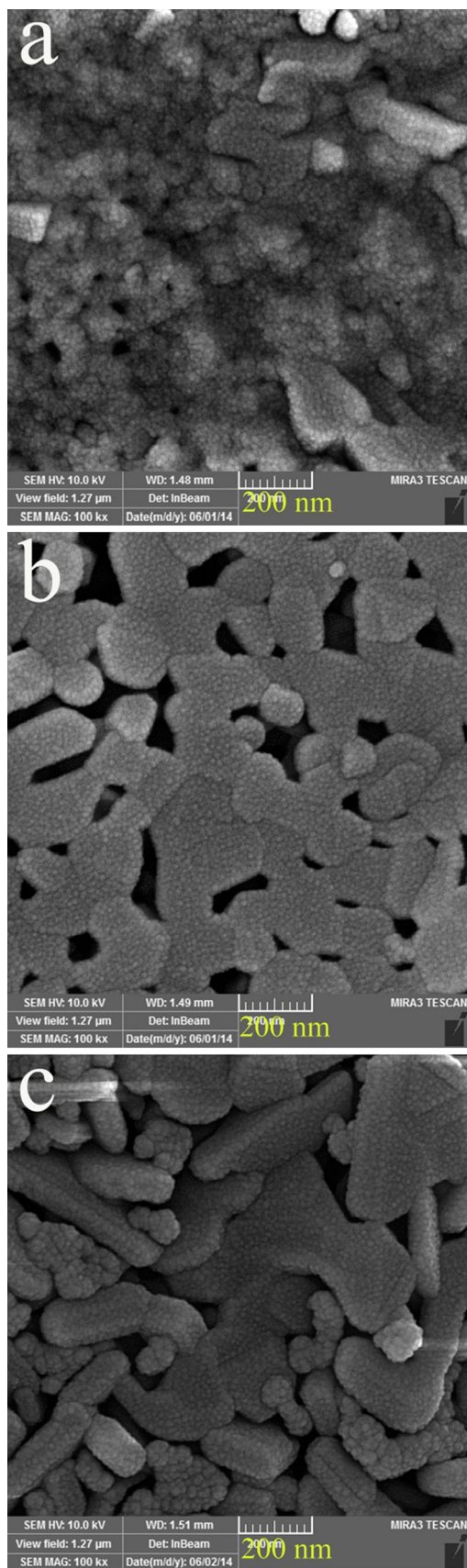


**Fig. 6** SEM images of the samples prepared by thermal treatment of Nd(III) complex in molar ratio of 1:1 at **a** 800 and **b** 900 °C

physisorbed water molecules linked to  $\text{Nd}_2\text{O}_3$  product [21]. The characteristic peak of  $\text{Nd}_2\text{O}_3$  seen at  $504\text{ cm}^{-1}$  is related to Nd–O vibration [22] (Fig. 1c). As can be seen, FT-IR results demonstrated the (L) Schiff base ligand, Nd(III) complex and neodymium oxide formation.

In order to investigate the thermal observation of the as-synthesized Nd(III) complex, thermal gravimetric analysis (TGA) was performed. The TGA curve of the as-prepared



◀**Fig. 7** SEM images of the products prepared from Nd(III) complex in molar ratios of **a** 1:0.5, **b** 1:1, and **c** 1:2, by thermal treatment of precursor at 900 °C for 5 h

Nd(III) complex is presented in Fig. 2. As seen in Fig. 2, there are three weight loss steps. The first weight loss happens in the temperature range 60–120 °C, and exhibits 2.1 % weight loss, which corresponds to surface moisture evaporating. The second step happens at the temperature range 120–430 °C (displaying 39.43 % weight loss), which may be ascribed to the loss of the (L) ligand. The third step happens in the temperature range 430–900 °C (displaying 32.95 % weight loss), which corresponds to the loss of two and one nitrate species from the inner and the outer coordination sphere of the as-synthesized Nd(III) complex, respectively, and the formation of neodymium oxide.

To characterize the composition and crystal structure of the as-prepared samples, XRD analysis was carried out (Fig. 3; Table 2). Figure 3a–c reveals the XRD pattern of samples synthesized at 700, 800 and 900 °C for 5 h (sample nos. 3–5). XRD results indicate that the samples synthesized through calcination at 700 and 800 °C consist of the cubic Nd<sub>2</sub>O<sub>3</sub> and NdO<sub>2</sub> and that the pure hexagonal Nd<sub>2</sub>O<sub>3</sub> has not been prepared (Fig. 3a, b). By increasing the temperature, pure hexagonal Nd<sub>2</sub>O<sub>3</sub> has been formed. All diffraction peaks in the XRD pattern (Fig. 3c) can be indexed to the pure hexagonal phase of Nd<sub>2</sub>O<sub>3</sub> (JCPDS Card file no. 74-2139). Utilizing Scherrer equation [23], the crystallite size of the synthesized Nd<sub>2</sub>O<sub>3</sub> from the XRD results was estimated to be about 28 nm. So, pure hexagonal Nd<sub>2</sub>O<sub>3</sub> can be prepared by calcining the obtained Nd(III) complex powder at 900 °C.

In order to further confirm the composition and purity of the as-prepared Nd<sub>2</sub>O<sub>3</sub>, EDS spectrum was obtained for Nd<sub>2</sub>O<sub>3</sub> synthesized by thermal treatment of Nd(III) complex in molar ratio of 1:1 at 900 °C. In the EDS spectrum of this sample (Fig. 4), Nd and O elements are observed. Therefore, the obtained XRD and X-ray microanalysis (EDX) results show that cubic hexagonal Nd<sub>2</sub>O<sub>3</sub> nanostructures were successfully synthesized through the present synthetic route.

To examine the influence of calcination temperature on the particle size and morphology of the Nd<sub>2</sub>O<sub>3</sub>, SEM images of Nd(III) complexes calcined at 500, 600, 700, 800 and 900 °C were taken and exhibited in Figs. 5 and 6, respectively. Obviously, 500, 600 and 700 °C are not the required temperature for decomposition of solid complex molecular precursor and no nanoparticle is formed (Fig. 5a–c). As the temperature is increased, agglomerated nanoparticles (sample nos. 4 and 5) are formed at 800 and 900 °C (Fig. 6a, b). As seen in Fig. 6a, b, by increasing the

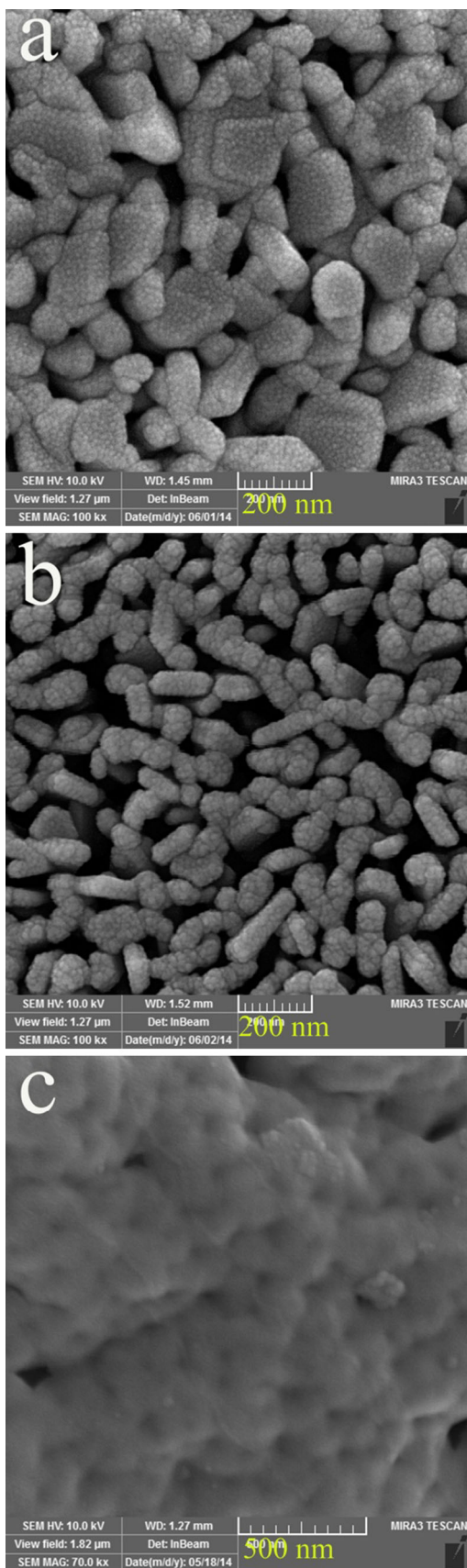


**Fig. 8** SEM images of the samples prepared from Nd(III) complex in molar ratios of **a** 1:3 and **b** 1:4, by thermal treatment of precursor at 900 °C for 5 h and **c** SEM image of Nd<sub>2</sub>O<sub>3</sub> prepared in the absence of Schiff base ligand

calcination temperature to 900 °C, the grain size of particles and the amount of the aggregates becomes larger. Therefore, the treatment temperature plays a significant role to control particle size and morphology of Nd<sub>2</sub>O<sub>3</sub>.

To investigate the influence of (L) Schiff base ligand amount on the morphology of the Nd<sub>2</sub>O<sub>3</sub>, experiments have been carried out by different molar ratios of Nd(NO<sub>3</sub>)<sub>3</sub>·6H<sub>2</sub>O to (L) (Table 1). Figures 7 and 8a, b demonstrate FESEM images of the Nd<sub>2</sub>O<sub>3</sub> obtained from Nd(III) complexes in the Nd(NO<sub>3</sub>)<sub>3</sub>·6H<sub>2</sub>O to (L) molar ratios of 1:0.5, 1:1, 1:2, 1:3 and 1:4, prepared via the solid state route and calcined at 900 °C for 5 h. As before described, privilege of this investigation is application of a new Schiff-base as complexing and capping agent for synthesis of Nd<sub>2</sub>O<sub>3</sub> nanostructures. This prepared Schiff-base has high steric hindrance and is a proper capping agent for preparing of nanostructures (Scheme 2). It seems that Schiff-base group due to its high steric hindrance effect causes nucleation to be happened rather than the growth. In our investigation, different molar ratios of Nd(NO<sub>3</sub>)<sub>3</sub>·6H<sub>2</sub>O to (L) were utilized to examine (L) amount influence on Nd<sub>2</sub>O<sub>3</sub> morphology. From the FESEM images, it can be observed that by utilizing molar ratio of 1:0.5 [Nd(NO<sub>3</sub>)<sub>3</sub>·6H<sub>2</sub>O to (L)], the nanoparticles are not form well (samples no. 6). With increase of (L) content (samples no. 7), with molar ratio of 1:1 [Nd(NO<sub>3</sub>)<sub>3</sub>·6H<sub>2</sub>O to (L)], agglomerated uniform spherical nanoparticles form (Fig. 7a, b). By increasing the molar ratio from 1:1 to 1:4, plate-like and bundle-like, and not uniform bundle-like Nd<sub>2</sub>O<sub>3</sub> nanostructures (sample nos. 7 and 8) as well as separated uniform mulberry-like nanostructures (sample no. 9) were obtained, respectively (Figs. 7c, 8a, b). It seems that when (L) amount increases, the aggregation between Nd<sub>2</sub>O<sub>3</sub> nanoparticles decreases due to steric hindrance effect of (L). Furthermore, images demonstrate that the particle size of Nd<sub>2</sub>O<sub>3</sub> decreases with decreasing Nd(NO<sub>3</sub>)<sub>3</sub>·6H<sub>2</sub>O to (L) molar ratio. It seems that when (L) content increases, nucleation to be happened rather than the particle growth due to steric hindrance effect of (L). Therefore, the molar ratio of Nd(NO<sub>3</sub>)<sub>3</sub>·6H<sub>2</sub>O to (L) has a great impact on the control of the particle size and morphology of Nd<sub>2</sub>O<sub>3</sub> nanostructures.

To study the influence of the (L) Schiff base ligand on the morphology, sample no. 10 was prepared as blank sample without applying any (L) at 900 °C. Figure 8c exhibits SEM image of sample no. 10. It can be observed that in the absence of Schiff base ligand, bulk structures were formed. This result demonstrate that applying (L) Schiff

**Scheme 2** Schematic diagram illustrating the formation of  $\text{Nd}_2\text{O}_3$  samples at various conditions

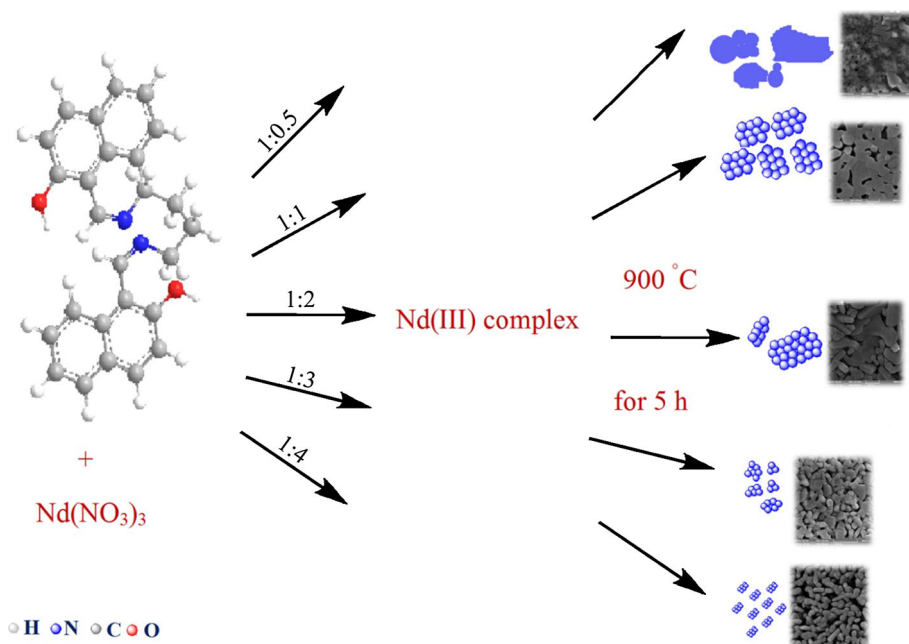
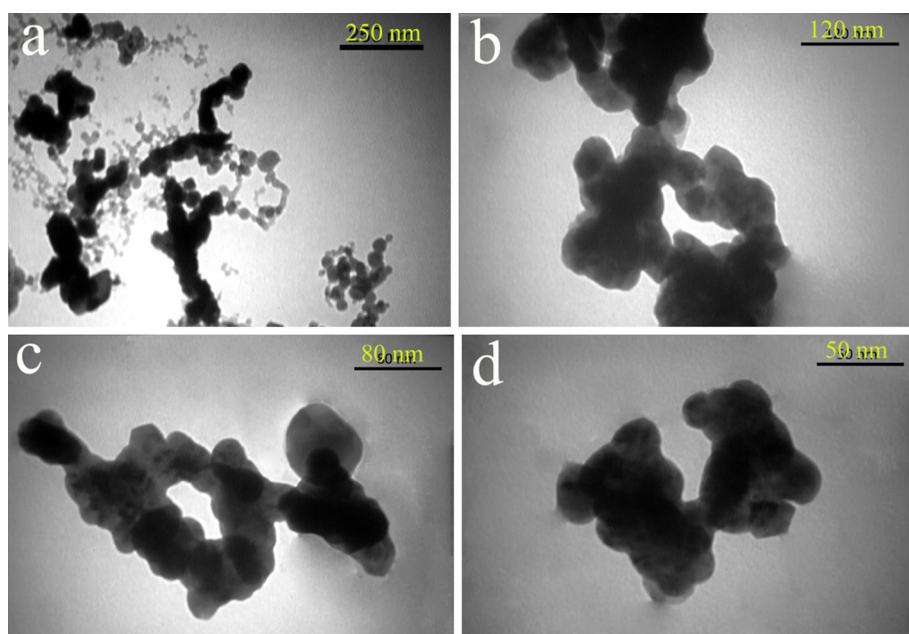


**Fig. 9** TEM images of nanostructured  $\text{Nd}_2\text{O}_3$  obtained by thermal treatment of Nd(III) complex in molar ratio of 1:4 at  $900\text{ }^\circ\text{C}$  for 5 h



base ligand with high steric hindrance led to prepare nanostructured  $\text{Nd}_2\text{O}_3$  at  $900\text{ }^\circ\text{C}$ , and we find out that huge ligands may be utilized instead of usual capping agents to control the morphology and particle size.

The size and morphology of as-obtained nanostructured  $\text{Nd}_2\text{O}_3$  were assessed with transmission electron microscopy (TEM) measurement. The typical TEM images (Fig. 9a–d) of the nanostructured  $\text{Nd}_2\text{O}_3$  in a molar ratio 1:4 [ $\text{Nd}(\text{NO}_3)_3 \cdot 6\text{H}_2\text{O}$  to (L)] are exhibited. The TEM images of the  $\text{Nd}_2\text{O}_3$  illustrate that quasi-spherical nanoparticles are sintered together. Furthermore, the images

demonstrate that as-formed nanoparticles have size in the range of 20–50 nm.

It is well known that the band gap ( $E_g$ ) plays a key role in characterizing the nanostructured materials properties utilized in photocatalytic applications and is oftentimes determined from the UV–Vis diffuse reflectance spectrum. Figure 10a exhibits the UV–Vis diffuse reflectance spectrum of the nanostructured  $\text{Nd}_2\text{O}_3$  in a molar ratio 1:1 [ $\text{Nd}(\text{NO}_3)_3 \cdot 6\text{H}_2\text{O}$  to (L)]. In the UV–Vis diffuse reflectance spectrum of the sample (Fig. 10a), the eight absorption bands (seen at 438, 482, 534, 596, 644, 694, 760 and



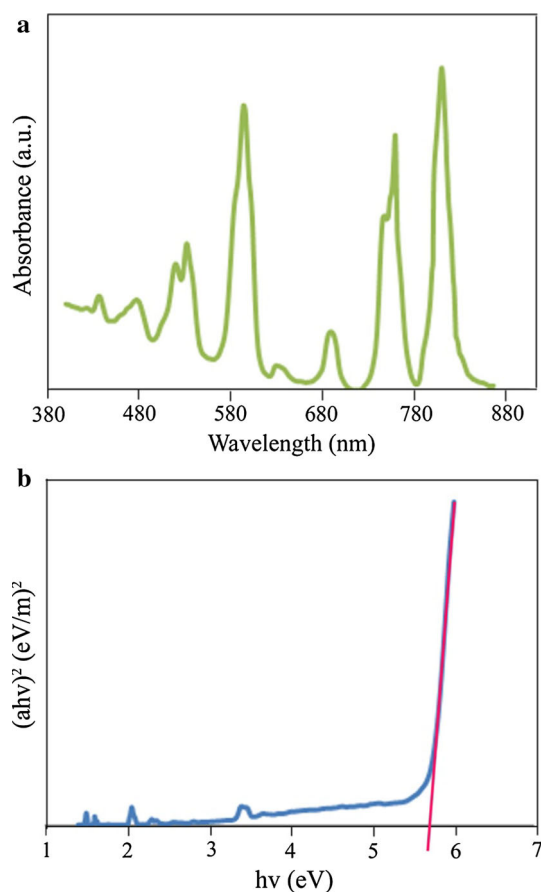


**Fig. 10** UV–Vis diffuse reflectance spectrum **a** and plot to determine the band gap **b** of the  $\text{Nd}_2\text{O}_3$  obtained by thermal treatment of Nd(III) complex in molar ratio of 1:1 at 900 °C for 5 h

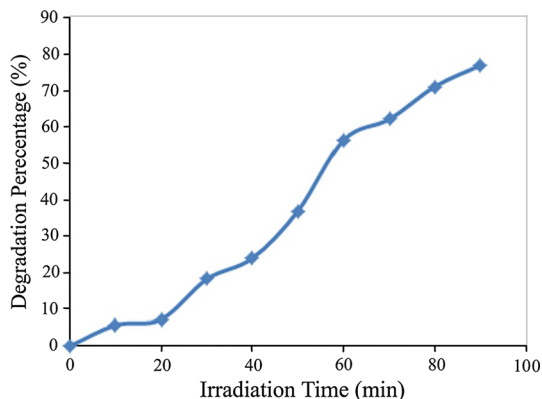
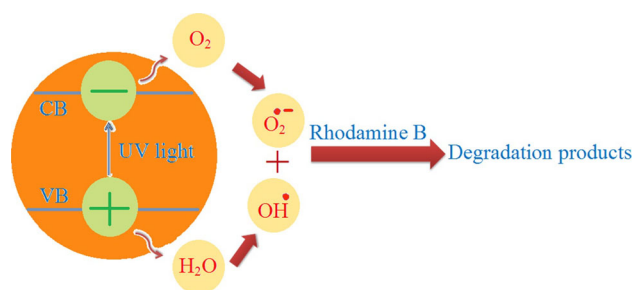


**Fig. 11** Photocatalytic rhodamine B degradation of  $\text{Nd}_2\text{O}_3$  nanoparticles obtained by thermal treatment of Nd(III) complex in molar ratio of 1:1 under UV light

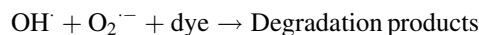
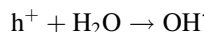
810 nm) are attributed to charge transition from  $^4I_{9/2}$  to  $^2G_{9/2} + ^2D_{3/2} + ^4G_{11/2} + ^2K_{15/2}$ ,  $^4G_{9/2} + ^4G_{7/2} + ^2K_{13/2}$ ,  $^4G_{5/2} + ^2G_{7/2}$ ,  $^2H_{11/2}$ ,  $^4F_{9/2}$ ,  $^4F_{7/2} + ^4S_{3/2}$ ,  $^4F_{5/2} + ^2H_{9/2}$  and  $^4F_{3/2}$ , respectively [24]. The (Eg) can be determined



**Scheme 3** Reaction mechanism of rhodamine B photodegradation over  $\text{Nd}_2\text{O}_3$  nanoparticles under UV light irradiation

based on the UV–Vis diffuse reflectance spectrum utilizing Tauc's relationship [25]. The (Eg) of the  $\text{Nd}_2\text{O}_3$  as direct semiconductor was obtained by extrapolating the linear portion of the plot of  $(\alpha h\nu)^2$  against  $h\nu$  to the energy axis (Fig. 10b). The obtained Eg value of the as-synthesized nanostructured  $\text{Nd}_2\text{O}_3$  estimated to be 5.75 eV, that has a blue shift compared with the obtained band gap amount of the  $\text{Nd}_2\text{O}_3$  in previous report [26] which this occurred blue shift is related to reduce in the particle size which this particle size reduction brings about variation in particle energy surfaces and enhance the band gap amount.

The photocatalytic activity of the nanostructured  $\text{Nd}_2\text{O}_3$  (sample no. 5) was examined by monitoring the photooxidation of rhodamine B as cationic dye in an aqueous solution, under UV light irradiation (Fig. 11; Scheme 3). No rhodamine B was practically broken down after 90 min without using UV light irradiation or nanostructured  $\text{Nd}_2\text{O}_3$ . This observation demonstrated that the contribution of self-degradation was insignificant. The probable mechanism of the photocatalytic degradation of cationic dye can be assumed as:



According to photocatalytic calculations by Eq. (1), the rhodamine B photooxidation was about 77 % after 90 min irradiation of UV light, and as-synthesized nanostructured  $\text{Nd}_2\text{O}_3$  demonstrated high photocatalytic activity. It has been shown that the heterogeneous photocatalytic processes comprise diffusion, adsorption and reaction steps, and proper distribution of the pore is effective and useful to diffusion of reactants and products, which prefer the photocatalytic reaction. In this study, the enhanced photocatalytic activity may be attributed to favorable distribution of the pore, high hydroxyl amount and high separation rate of charge carriers [27].

## 4 Conclusions

Nanostructured  $\text{Nd}_2\text{O}_3$  with different morphologies was successfully prepared through a new and facile route. First, solid complex molecular precursor  $[\text{Nd L}(\text{NO}_3)_2]\text{NO}_3$  (L = bis-(2-hydroxy-1-naphthaldehyde)-butanediamine Schiff base ligand) was successfully prepared by a mechano-chemical solid–solid route, and then nanostructured  $\text{Nd}_2\text{O}_3$  was obtained by thermal treatment of  $[\text{Nd L}(\text{NO}_3)_2]\text{NO}_3$  at 900 °C for 5 h. In this study solid state route coupled with thermal treatment in the absence of any other template or surfactant, is considered a reliable, reproducible, simple and practical method with several advantages such as saving of time and energy, free from utilizing organic solvent and ease of controlling reaction temperature, all of which contribute to large-scale production. Various techniques including EDS, XRD, FT-IR, FESEM, UV–Vis diffuse reflectance spectroscopy, and TEM were applied to characterize the structural and optical properties of the as-obtained nanostructures. The synthesized nanostructured  $\text{Nd}_2\text{O}_3$  can be utilized as an interesting candidate for photocatalytic applications under UV light such as removal of rhodamine B as cationic dye, since the degradation percentage of the rhodamine B was found to be 77 within 90 min.

**Acknowledgments** Authors are grateful to the Council of University of Kashan for providing financial support to undertake this work by Grant No. (159271/388).

## References

- H.Y. Xia, G.Q. He, Y.L. Min, T. Liu, J. Mater. Sci. Mater. Electron. **26**, 3357 (2015)
- G.V. Khade, M.B. Suwarakar, N.L. Gavade, K.M. Garadkar, J. Mater. Sci. Mater. Electron. **26**, 3309 (2015)
- S. Zinatloo-Ajabshir, M. Salavati-Niasari, J. Ind. Eng. Chem. **20**, 3313 (2014)
- A. Sobhani, M. Salavati-Niasari, J. Alloys Compd. **617**, 93 (2014)
- S. Zinatloo-Ajabshir, M. Salavati-Niasari, Int. J. Appl. Ceram. Technol. **11**, 654 (2014)
- A. Sobhani, M. Salavati-Niasari, J. Alloys Compd. **625**, 26 (2015)
- S. Zinatloo-Ajabshir, M. Salavati-Niasari, Ceram. Int. **41**, 567 (2015)
- T. Sreethawong, S. Chavadej, S. Ngamsinlapasathian, S. Yoshikawa, Solid State Sci. **10**, 20 (2008)
- R. Bazzi, M.A. Flores-Gonzalez, C. Louis, K. Lebbou, C. Dujardin, A. Brenier, W. Zhang, O. Tillement, E. Bernstein, P. Perriat, J. Lumin. **102**, 445 (2003)
- M. Zawadzki, L. Kępiński, J. Alloys Compd. **380**, 255 (2004)
- A. Kosola, J. Päiväsaari, M. Putkonen, L. Niinistö, Thin Solid Films **479**, 152 (2005)
- T. Liu, Y. Zhang, H. Shao, X. Li, Langmuir **19**, 7569 (2003)
- F. Delmore, C. Harnois, I. Monot-Laffez, G. Desgardin, Phys. C **372**, 1127 (2002)
- W. Zhu, J. Ma, L. Xu, W. Zhang, Y. Chen, Mater. Chem. Phys. **122**, 362 (2010)
- C.R. Michel, A.H. Martinez-Preciado, N.L. Lopez Contreras, Sens. Actuators B **184**, 8 (2013)
- S.V. Chavan, P.U.M. Sastry, A.K. Tyagi, J. Alloys Compd. **456**, 51 (2008)
- L. Kępiński, M. Zawadzki, W. Miśta, Solid State Sci. **6**, 1327 (2004)
- Q. Liqin, W. Kaituo, W. Xuehang, W. Wenwein, L. Sen, L. Gengming, Ceram. Int. **40**, 3003 (2014)
- S.M. Kaczmarek, G. Leniec, J. Non Cryst. Solids **355**, 1325 (2009)
- K. Binnemans, Y.G. Galyametdinov, R. Van Deun, D.W. Bruce, S.R. Collinson, A.P. Polishchuk, J. Am. Chem. Soc. **122**, 4335 (2000)
- Y.L. Zhang, W.W. Qin, W.S. Liu, M.Y. Tan, N. Tang, Spectrochim. Acta A **58**, 2153 (2002)
- L.M. Sharaf El-Deen, M.S. Al Salhi, M.M. Elkholy, J. Alloys Compd. **465**, 333 (2008)
- R.L. Snyder Jenkins, *Chemical Analysis: Introduction to X-ray Powder Diffractometry* (Wiley, New York, 1996), pp. 89–91
- R. Bazzi, A. Brenier, P. Perriat, O. Tillement, J. Lumin. **113**, 161 (2005)
- M. Salavati-Niasari, D. Ghanbari, M.R. Loghman-Estarki, Polyhedron **35**, 149 (2012)
- A.V. Prokofiev, A.I. Shelykh, B.T. Melekh, J. Alloys Compd. **242**, 41 (1996)
- J. Zhong, J. Li, F. Feng, Y. Lu, J. Zeng, W. Hu, Z. Tang, J. Mol. Catal. A Chem. **357**, 101 (2012)